ISSN 1547-4771, Physics of Particles and Nuclei Letters, 2019, Vol. 16, No. 1, pp. 21–29. © Pleiades Publishing, Ltd., 2019.
Russian Text © A.V. Bogomyagkov, S.A. Glukhov, K.Iu. Kariukina, O.S. Kozlov, S.A. Kostromin, E.B. Levichev, N. Carmignani, S.M. Liuzzo, 2019, published in Pis'ma v Zhurnal Fizika Elementarnykh Chastits i Atomnogo Yadra, 2019.

PHYSICS AND TECHNIQUE OF ACCELERATORS

Dynamic Aperture of the NICA Collider Optimized with a Genetic Algorithm

A. V. Bogomyagkov[a], S. A. Glukhov[a], K. Iu. Kariukina[a, *], O. S. Kozlov[b], S. A. Kostromin[b], E. B. Levichev[a], N. Carmignani[c], and S. M. Liuzzo[c]

[a] *Budker Institute of Nuclear Physics, Novosibirsk, 630090 Russia*
[b] *Joint Institute for Nuclear Research, Dubna, Moscow oblast, 141980 Russia*
[c] *European Synchrotron Radiation Facility, Grenoble, 38000 France*
**e-mail: kskaryukina@gmail.com*

Received July 12, 2018

Abstract—NICA (Nuclotron-based Ion Collider fAcility) [1] is a heavy-ion collider for studying the properties of hot and dense baryonic matter to be constructed at JINR (Dubna). A major restricting factor on the NICA's transverse dynamic aperture is the nonlinear fringe field of final-focus quadrupole lenses. We propose to enhance the NICA dynamic aperture with a set of multipole lenses whose characteristics and configuration are optimized using a genetic algorithm.

DOI: 10.1134/S1547477119010060

INTRODUCTION

The NICA facility will allow for a variety of experiments with colliding beams of different particles ranging from protons and polarized deuterons to massive gold ions. The collider consists of two storage rings placed one above the other; the beams are separated in the vertical plane by bending magnets with a length of 1.4 m and bending angle of 40 mrad.

Each storage ring follows the racetrack scheme and is formed by two arcs and two straight sections where the detectors, RF stations, and electron and stochastic cooling systems are deployed. The straight sections also house two triplets of final-focus quadrupole lenses; separating magnets; beam-correcting magnets, including nonlinear ones; and some other equipment. Each bending ark consists of 12 regular FODO cells [2]. Optical functions of the ring as a whole and of the final focus computed with the Accelerator Toolbox (AT) package for the NICA-ring-8 structure [3] are shown in Figs. 1 and 2. The total circumference of the NICA storage ring amounts to 503 m. Betatron functions are tuned to 60 cm at the collision point, reaching a maximum of 135 m in the central final-focus lens. The values of major storage-ring parameters assumed in simulating the beam dynamics are listed in Table 1. Beam magnetic rigidity reaches a maximum value of $B\rho = 45$ T m for ^{79}Au ions accelerated to 4.5 GeV/nucleon.

Since the ring includes solenoids (see Table 2, where $\varphi = eB/p_0c$), selecting the working point near the difference resonance gives rise to coupled betatron oscillations, which significantly affect particle dynamics.

In studying the beam dynamics and optimizing the dynamic aperture, we rely on the Accelerator Toolbox (AT) simulation package [4]. The validity of AT predictions is confirmed by additional simulations carried out with the TrackKing [5] and MADX [6] program packages.

1. ORIGINAL DYNAMIC APERTURE

The dynamic aperture (DA) is defined as an area of the six-dimensional phase space in which particle motion remains stable under nonlinear perturbations. The DA is an important characteristic of a cyclic accelerator which determines the beam lifetime and the efficiency of beam injection. Following the simplest and most widely accepted approach, we define the DA as the area of initial particle coordinates $z_0(x_0)$, $x_0' = z_0' = 0$ for which the particle motion remains stable upon a certain number of revolutions (2^{10} for the discussed case) given a certain fixed value or relative momentum $\delta = \Delta p/p$. In this paper, our aim consists of enhancing and optimizing the dynamic aperture. Towards this, we perform multiple trials assigning different values to the strengths of nonlinear magnetic elements, betatron frequencies, and particle momenta and then compare their results. Since these multiple trials consume a large amount of processor time, we aim at minimizing the DA computation time for each trial by using the simplest DA definition. In order to

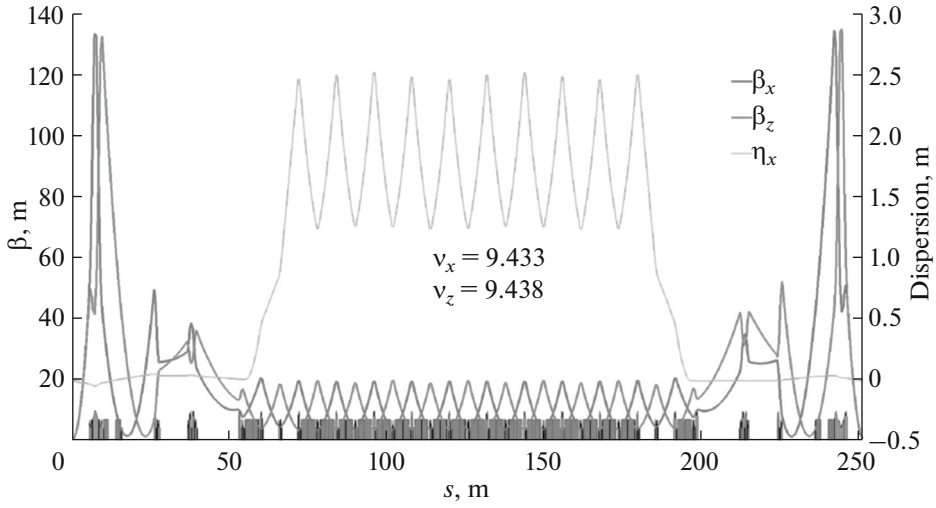

Fig. 1. Twiss functions for half of the NICA ring.

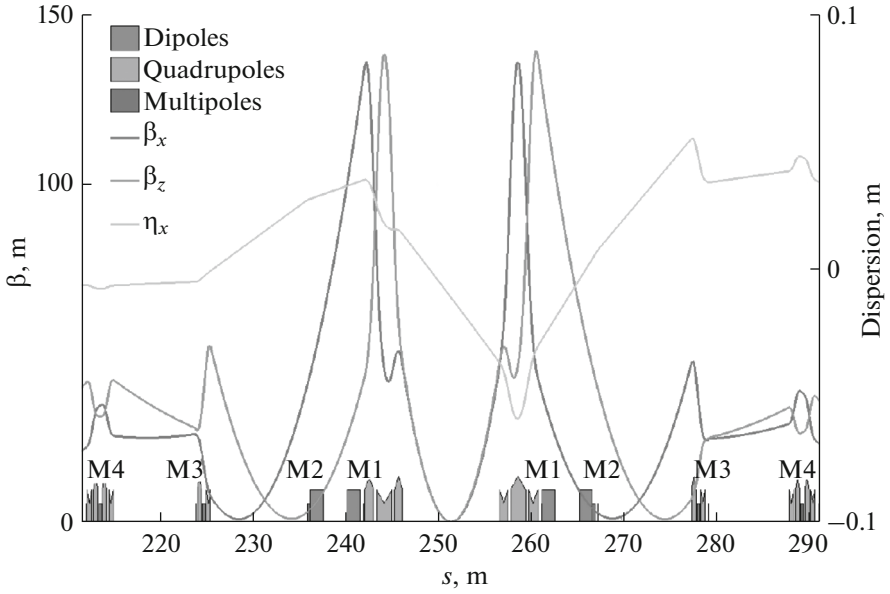

Fig. 2. Twiss functions for the NICA final focus.

minimize the processor time required for the simulation, we purposefully forgo the more rigorous but time-consuming DA definitions and leave out those that refer to a smaller number of turns (>1000) and the total duration of an experiment [7].

The effects of nonlinear perturbations arising from the sextupole magnets correcting for the natural chromaticity and from fringe fields of quadrupole lenses on the NICA DA were analyzed in [8]. Note that, for a circulating beam with equilibrium transverse dimensions, the DA is largely restricted by the fringe field of the final-focus triplet of lenses with large values of beta-functions rather than by those of quadrupole lenses placed in the arcs. The DA of the NICA collider, estimated either neglecting or considering the nonlinear fringe fields of quadrupole lenses, is shown in Fig. 3. Natural chromaticity is corrected for with four sets of sextupole lenses deployed in bending arcs near the maxima of betatron functions corresponding to the FODO structure. The required numbers of different sextupole lenses and their parameters for $B\rho$ = 45 T m are listed in Table 3.

The dynamic aperture shown in Fig. 3 is estimated as $A_{x,z} \approx 13\sigma_{x,z}$ if fringe fields are neglected, and as $A_{x,z} \approx 7\sigma_{x,z}$ if they are considered. Fringe fields are seen to effectively reduce the aperture down to the storage-ring geometric acceptance (or nearly by a fac-

Table 1. Basic parameters of the NICA storage ring

Circumference, m	503.04
Number of bunches	22
Bunch rms length, m	0.6
β function at collision point, m	0.597/0.601
Betatron frequencies, Qx/Qz	9.43/9.44
Natural chromaticity, $Q'x/Q'z$	−23.8/−23.9
Ring acceptance, π mm mrad	40
Momentum acceptance, $\Delta p/p_{\max}$	±0.010
Critical energy, γ_{tr}	7.088
Energy of ^{79}Au ions, GeV/nucleon	4.5
Number of ions per bunch	2.3×10^{9}
rms momentum spread $\Delta p/p$	1.5×10^{-3}
rms emittance, π mm mrad	1.1/0.75
Peak luminosity, $\mathrm{cm}^{-2}\,\mathrm{s}^{-1}$	1.0×10^{27}

Table 2. Parameters of the solenoids entering the NICA ring structure

Solenoid location	Length L, m	φ, rad/m
SPD detector	10.5	0
MPD detector	10.5	0.0112
Electron cooling system	6	0.0045

Table 3. Parameters of the sextupole lenses correcting for natural achromaticity

Lens	N	$B''L/B\rho$, m^{-2}
SF1	8	0.619
SD1	8	−1.023
SF2	8	0.316
SD2	8	−0.819

tor of two). Figure 4 shows the betatron-oscillation frequency as a function of the particle amplitude. The contribution of lens edges to the frequency increment is always positive irrespective of the quadrupole-lens polarity [9] and significantly exceeds that of chromatic sextupoles. Since the unperturbed frequency is selected to lie slightly below the half-integer resonance, increasing the oscillation amplitude shifts the horizontal and vertical frequencies, which may result in a particle loss at the half-integer resonance. In Fig. 4, $\nu_z(x)$ is plotted for a minimal vertical amplitude of 30 μm.

2. FRINGE FIELD OF A QUADRUPOLE LENS

Effects of the nonlinearity of quadrupole-lens fringe field on beam dynamics have been analyzed elsewhere [10–15]. In the leading order, the particle-motion Hamiltonian considering the quadrupole and octupole nonlinearities has the form [14]

$$H = \frac{1}{2}(p_x^2 + p_z^2) + \frac{1}{4}k_1'(p_x x z^3 - p_z z x^3) - \frac{1}{48}k_1''(x^4 - z^4) + \frac{1}{24}k_3(x^4 - 6x^2z^2 + z^4), \quad (1)$$

where $k_1 = (dB_z/dx)/B\rho$ is the reduced focusing coefficient, $k' = (dk/ds)/B\rho$ is the derivative of gradient variation at the lens edge, and $k_3 = (d^3 B_z/dx^3)/B\rho$ is the octupole nonlinearity. In (1), the first term

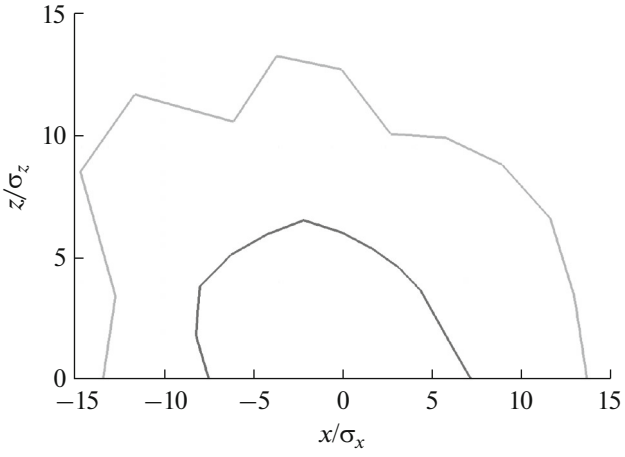

Fig. 3. Effect of quadrupole-lens fringe fields on the dynamic aperture. The dynamic aperture is simulated either neglecting the edge effects (light gray line) or taking them into account (dark gray line).

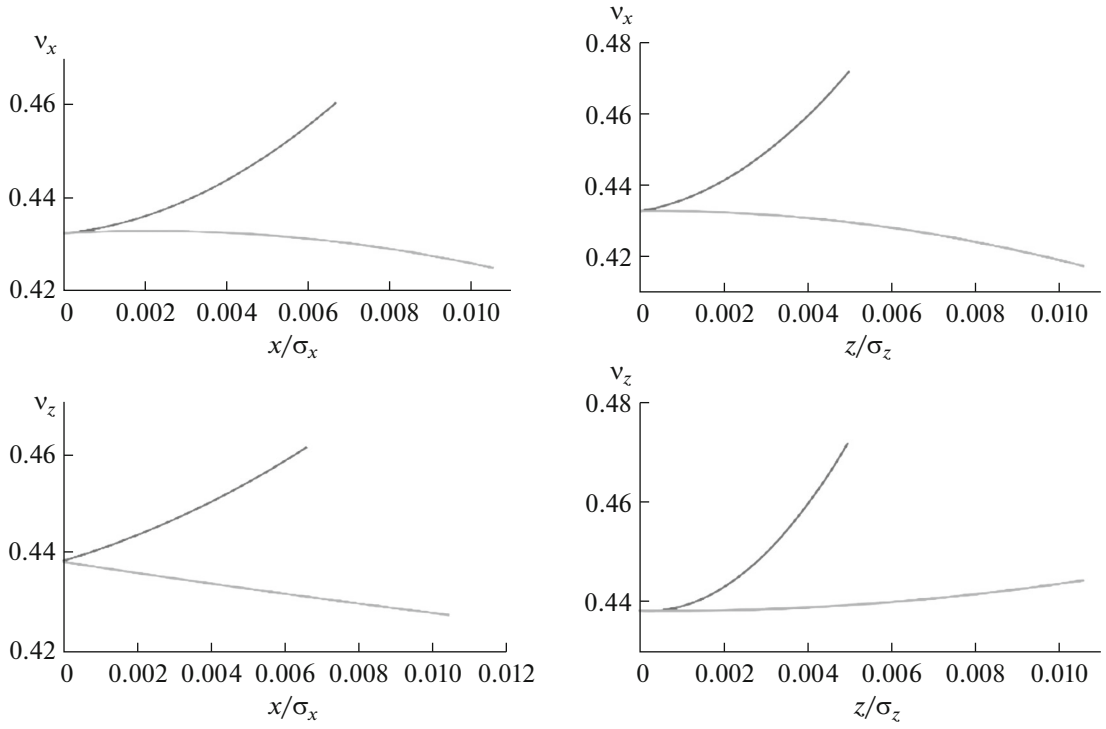

Fig. 4. Horizontal and vertical betatron frequencies as functions of the amplitudes plotted neglecting the edge effects (light gray line) and taking them into account (dark gray line).

describes linear motion, the second and third terms describe the effect of the quadrupole-lens fringe field, and the last term is the octupole-lens contribution. Note that, in [16], the Hamiltonian has a different form, since an alternative gauge is selected for the vector potential of electromagnetic field. However, since the equations of motion are invariant with respect to the gauge, for both Hamiltonian forms we have

$$\begin{aligned} x'' &= -k_1(x - x'z'z + \frac{3}{2}xx'^2 + \frac{1}{2}xz'^2) \\ &+ \frac{1}{12}k_1''(x^3 + 3xz^2) + k_1'xzz' + \frac{1}{6}k_3(x^3 - 3xz^2), \\ z'' &= k_1(z - x'z'x + \frac{3}{2}zz'^2 + \frac{1}{2}zx'^2) \\ &- \frac{1}{12}k_1''(z^3 + 3zx^2) - k_1'zxx' + \frac{1}{6}k_3(z^3 - 3zx^2). \end{aligned} \tag{2}$$

In Eq. (2), the leading term of the perturbation arising from the fringe-field and octupole nonlinearities involves monomes of the same fourth power in the variables. This suggests that the effect of the quadrupole-lens fringe field may be compensated by octupole correctors (since that of sextupole lenses is small). The problems posed by such a compensation can be elucidated by considering the shift of betatron-oscillation frequency in the first order of perturbation theory:

$$\begin{aligned} \Delta\nu_x &= a_{xx}J_x + a_{xz}J_z, \\ \Delta\nu_z &= a_{zx}J_x + a_{zz}J_z. \end{aligned} \tag{3}$$

Here, the action variables are defined as $x = \sqrt{2J_x\beta_x}\cos\phi_x$ and analogously for z, and the coefficients are expressed as [14]

$$\begin{aligned} a_{xx} &= \frac{1}{16\pi}\oint k_3\beta_x^2 ds - \frac{1}{32\pi}\oint k_1''\beta_x^2 ds, \\ a_{zx} &= a_{xz} = -\frac{1}{8\pi}\oint k_3\beta_x\beta_z ds \\ &+ \frac{1}{8\pi}\oint k_1'(a_z\beta_x - a_x\beta_z)ds, \\ a_{zz} &= \frac{1}{16\pi}\oint k_3\beta_z^2 ds + \frac{1}{32\pi}\oint k_1''\beta_z^2 ds, \end{aligned} \tag{4}$$

where $a_{x,z} = -\beta'_{x,z}/2$. It may seem that the nonlinear effect induced by quadrupole-lens edges can be locally mitigated by directly adding a cubic component to the quadrupole-lens field. If the lens provides a moderate focusing (or $L\sqrt{k_1} < 1$), Eq. (4) can be significantly simplified by approximating the magnetic field with a step function so that the integral reduces to a sum over magnets [14]:

$$\begin{aligned} a_{xx} &\approx \frac{1}{16\pi}\sum_i (k_3\overline{\beta_x^2}L)_i + \frac{1}{8\pi}\sum_i (k_1^2\overline{\beta_x^2}L)_i, \\ a_{zx} &= a_{xz} \approx \frac{-1}{8\pi}\sum_i (k_3\overline{\beta_x\beta_z}L)_i \\ &+ \frac{1}{4\pi}\sum_i (k_1^2\overline{\beta_x\beta_z}L)_i, \\ a_{zz} &\approx \frac{1}{16\pi}\sum_i (k_3\overline{\beta_z^2}L)_i + \frac{1}{8\pi}\sum_i (k_1^2\overline{\beta_z^2}L)_i, \end{aligned} \tag{5}$$

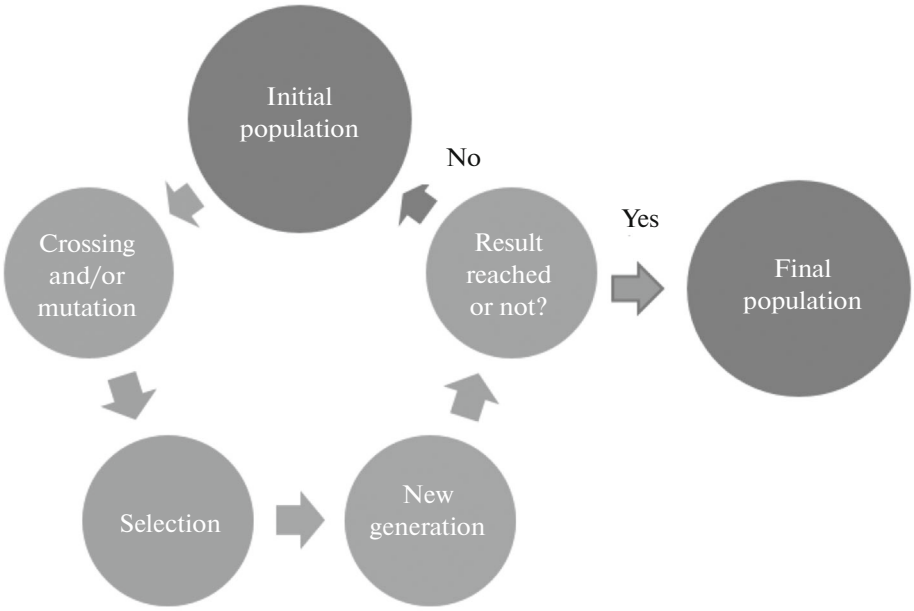

Fig. 5. Schematic representation of the genetic algorithm.

where betatron functions are averaged over the lens length. These equations demonstrate that the direct coefficients a_{xx} and a_{zz} can be canceled by introducing a cubic field component with a magnitude of $k_3 = -2k_1$. However, this effectively doubles the value of the a_{xz} coefficient and, therefore, is unlikely to result in increasing the dynamic aperture. For this reason, one has to employ more complex schemes involving octupole correctors. To conclude this section, we should indicate that, in the leading order, the transformation of particle coordinates across the first (or entrance) edge of a quadrupole lens has the following simple form [16]:

$$\begin{aligned} \Delta x &= -\frac{k_1}{12}(x^3 + 3xz^2), \\ \Delta p_x &= \frac{k_1}{4}((x^2 + z^2)p_x + 2xzp_z), \\ \Delta z &= \frac{k_1}{12}(z^3 + 3zx^2), \\ \Delta p_z &= -\frac{k_1}{4}((x^2 + z^2)p_z + 2zxp_x). \end{aligned} \quad (6)$$

This transformation is symplectic and has an opposite sign across the second (exit) edge of the lens.

3. GENETIC ALGORITHM

The DA of the NICA collider is optimized using the MATLAB NGPM code [17], which is an implementation of the NSGA-II algorithm (hence, its name which is an acronym of A NSGA-II Program in MATLAB). NSGA-II is a multicriterion genetic algorithm which offers an adaptive method for finding the optimal solution in the form of a maximum or minimum of a given aim function. Evolution simulation was pioneered by Niels Barricelli in 1954 [19, 20]. Genetic algorithms owe their popularity to John Holland's paper published in the early 1970s and to his subsequent monograph "Adaptation in Natural and Artificial Systems" [21]. The algorithm is rooted in the mechanisms of genetic heredity and natural selection of Darwin's evolution theory. For this reason, it is formulated in terms of biological origin. Thus, a trial solution of the optimization problem is referred to as a specimen or chromosome, and the set of all trial solutions at a given evolution stage a called a population. Genetic algorithms are largely targeted at resolving the problem of precocious convergence with the aim function reaching a local rather than global extremum.

At the first step, the genetic algorithm (see Fig. 5) forms the original population (the set of possible solutions) either randomly or using some probabilistic approach. Reaching the global optimum can be significantly accelerated by properly selecting the original population. Then, selection operators are used for selecting two parent solutions which, upon applying crossing operators, give rise to an offspring solution. This is then subjected to small random modifications (mutations) towards rejecting local minima. This breeding process is aimed at forming a new population of solutions which are closer to the global minimum than those of the preceding population. As in biological evolution, the strongest specimens survive: the nearly optimal solutions remain in the population, while those that are far from the optimum (the weak offspring) are rejected. The process is terminated as soon as the optimum solution is reached, the number

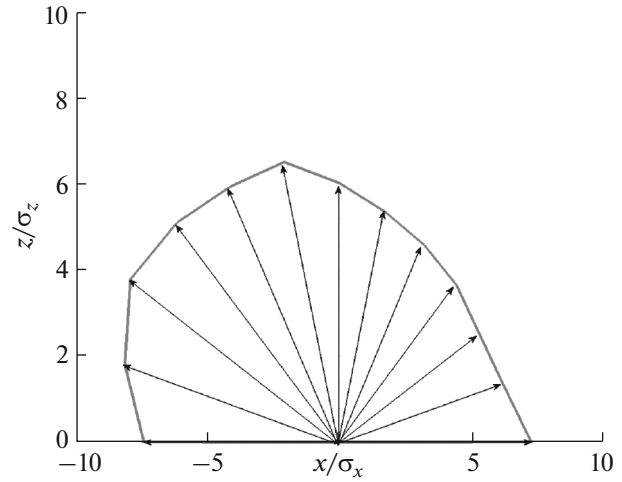

Fig. 6. Graphical representation of the technique for estimating the dynamic aperture.

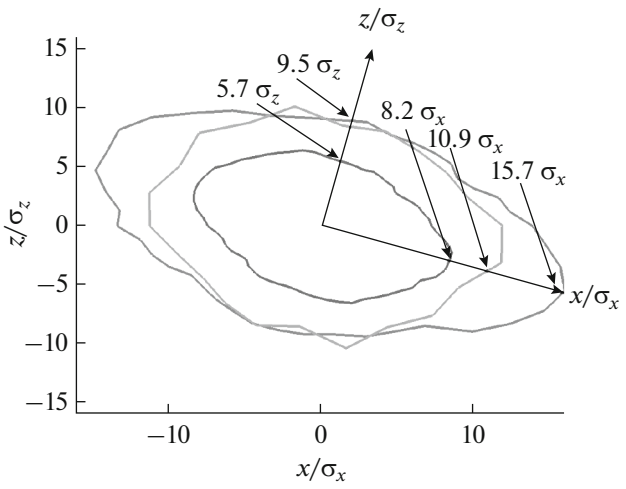

Fig. 7. Dynamic aperture of the NICA collider prior to optimization (blue contour) and upon optimization with two groups of octupole correctors M1 and M2 (green contour) and with four groups M1–M4 (red contour).

of the generation exceeds a certain maximum, or the available computer time expires.

The above description of the genetic approach is of course oversimplified. For an in-depth understanding of genetic algorithms used in accelerator physics, the reader is referred to [22–27]. Today, a number of computer codes with genetic algorithms aimed at simulating, developing, and optimizing particle accelerators are available.

4. ACCELERATOR TOOLBOX

The Accelerator Toolbox (AT) software package, aimed at designing and simulating both the cyclic accelerators and linear structures (such as beam-transport channels), was originally conceived by A. Terebilo [28]. This is achieved conveniently on the MATLAB platform [29], which is well known as a powerful commercially available package of applied programs addressing technical, physical, and mathematical problems. Apart from providing an interactive medium, MATLAB offers a high-level interpretable programming language used in the AT basic functions and procedures. The functions that require high-speed computations (such as particle tracking) are written with C/C++ and compiled to binary files run in the MATLAB medium. This approach is convenient, since a user can rely on the MATLAB's tested embedded software for editing and controlling the data, visualization, optimization, and processing the results of accelerator simulations (e.g., for computing the Fourier series needed for determining the frequencies of betatron oscillations) and no longer worry about exporting the data and matching different formats. The AT code is open and allows a user to add his own procedures and functions. Today, the people working on Accelerator Toolbox form a worldwide collaboration [30].

5. STRUCTURE OPTIMIZATION

Dynamic acceptance of the NICA collider is optimized using correcting octupole magnets M1–M4 deployed on the left and right sides of (each) collision point, as is shown in Fig. 2. Both the mirror-symmetric and asymmetric corrector forces with respect to the collision point were considered. For the arrangements with originally asymmetric forces, an approximate symmetry is always restored upon applying the optimization algorithm. Therefore, in what follows we restrict analysis to mirror-symmetric corrector arrangements, which require fewer power sources.

The DA size is optimized using 13 rays with a 15° angular pitch on the $z_0(x_0)$ plane as shown in Fig. 6, where both coordinates are normalized to corresponding rms beam dimensions $\sigma_{x,z}$.

The initial particle position from which the tracking through the magnetic structure begins moves along the beam with a given pitch towards the origin starting from large coordinate values, where particle motion is known to be unstable. The DA boundary in the given direction is estimated as the position of the first point for which the particle motion remains stable during 2^{10} revolutions. Owing to the uncompensated coupling between betatron oscillations, the axes of transverse-oscillation modes are slightly rotated with respect to those of the simulation program around the origin (collision azimuth), as is illustrated by Fig. 6. This effect will disappear upon the betatron-coupling correction and is anyway irrelevant to our task of enhancing the NICA's dynamic aperture. Still, an additional small tuning may be required upon correcting for the betatron coupling.

The results of our analysis are graphically shown in Fig. 7 and quoted in Table 4. In the vertical direction,

Table 4. Horizontal and vertical boundaries of the NICA dynamic aperture

Structure	Horizontal DA, σ_x	Vertical DA, σ_z
Original	8.2	5.7
Optimized with the M1 and M2 octupoles	10.9	8.8
Optimized with the M1–M4 octupoles	15.7	9.5

the apertures obtained with two and four correctors are approximately equal: $N\sigma_z \approx 9\sigma_z$. In the horizontal direction, optimization with four correctors M1–M4 yields a larger aperture than that with only two correctors M1 and M2 ($N\sigma_x \approx 15.7\sigma_x$ and $N\sigma_x \approx 10.9\sigma_x$, respectively). The latter could be an argument in favor of horizontal injection. Integrated strengths of octupole correctors corresponding to the optimized apertures shown in Fig. 7 are quoted in Table 5. The dependences of the betatatron-oscillation frequency on the initial particle coordinates, $\nu_{x,z}(x, z)$, prior to and upon optimization with the M1, M2 and M1–M4 correctors, are shown in Fig. 8. In the region of strong resonances, the beam particle is seen to lose stability either above the initial point at $\nu_{x,z}(x, z) \approx 9.44$ (most probably corresponding to the $\nu_{x,z}(x, z) \approx 9.5$ half-integer resonance) or below the initial point (presumably at $\nu_{x,z}(x, z) \approx 9.33$). The aperture size will benefit from restricting the frequencies of betatron oscillations to a certain band removed from these resonances. The momentum acceptance is not optimized since, as is demonstrated by Fig. 9, it exceeds the

Table 5. Integrated strengths of optimized octupole correctors

	M1	M2	M3	M4
$\frac{1}{6}\frac{1}{B\rho}\frac{d^3Bz}{dx^3}l$, m^{-3}	0.28	−8	–	–
$\frac{1}{6}\frac{1}{B\rho}\frac{d^3Bz}{dx^3}l$, m^{-3}	0.03	−5	0.92	1.41

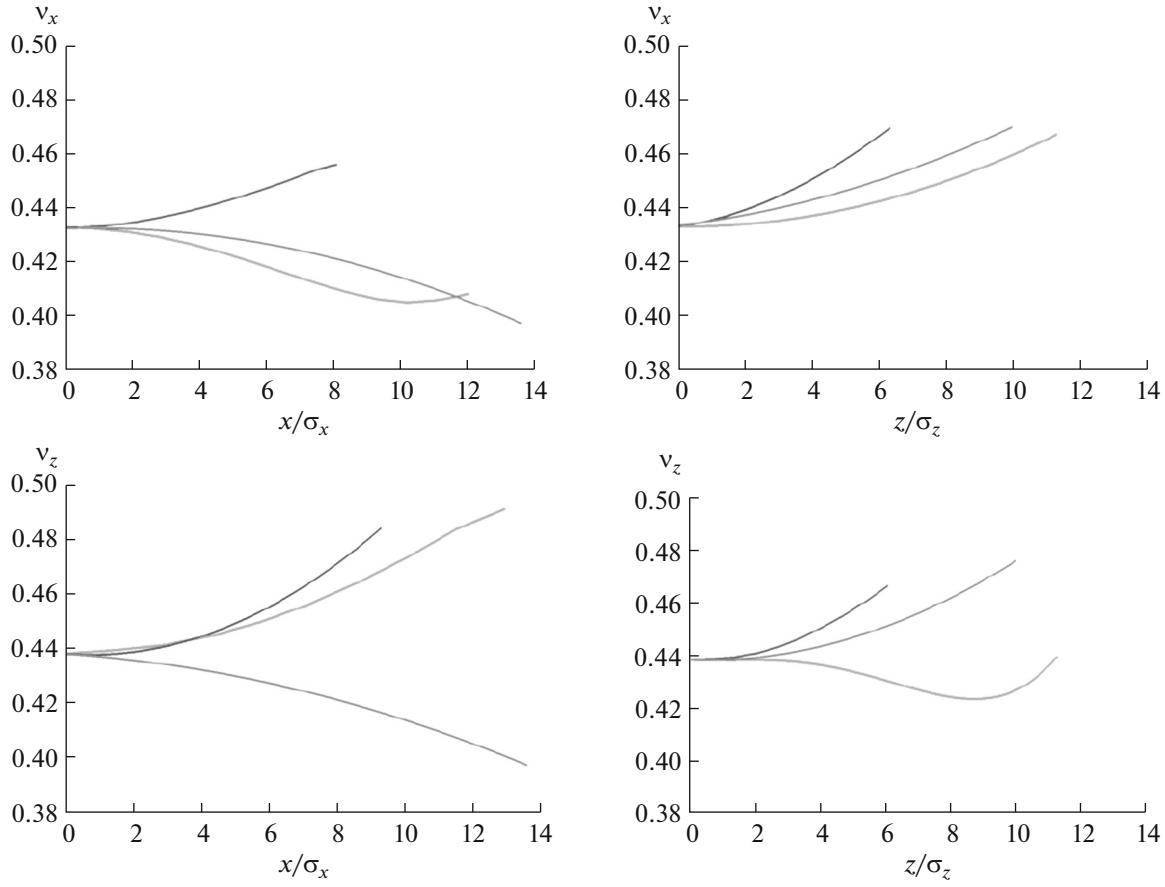

Fig. 8. Betatron frequencies as functions of transverse-oscillation amplitudes. The colors correspond to those in Fig. 7.

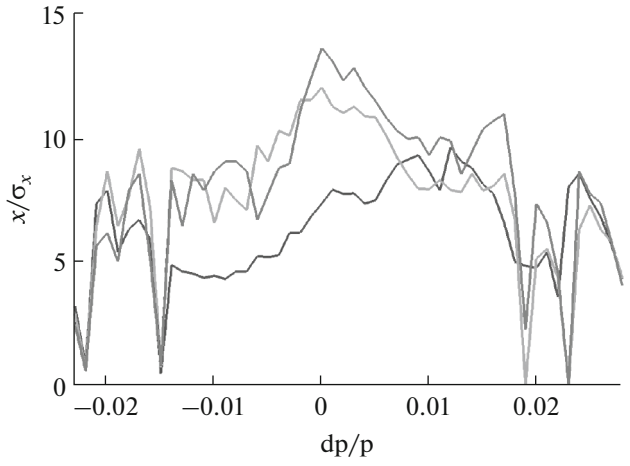

Fig. 9. Horizontal aperture as a function of beam-momentum smearing. The colors correspond to those in Fig. 7.

required ±1% for both the default structure and those featuring magnetic correctors. Prior to running the genetic algorithm, one should select the population size, mutation techniques, number of generations, etc. Though there exist no exact criteria for optimally selecting these parameters, some empirical recommendations are available. Thus, the population size should be selected as 50 if the number of variables is between two and five and 200 if this number is larger. The recommended number of generations is the number of variables multlplied by 100. If the solution shows a fast convergence but one suspects that the minimum is local rather than global, the mutation probability should be increased. Our parallel calculations rely on the four-nucleus processor Intel Core i7-4790 CPU 3.6 GHz. Simulating a single generation takes nearly 2640 s for two variables (147 h for 200 generations of 50 specimens) and 8700 s for six variables (60 days for 600 generations of 200 specimens). In most cases, tracking was performed for a smaller number of turns without significantly affecting the final results. We also attempted to minimize the number of octupole correctors required for increasing the aperture by relying on only two correctors closest to the collision point (M1 and M2) rather than on four ones.

CONCLUSIONS

We propose to enhance the transverse dynamic aperture of the NICA collider by installing sets of nonlinear octupole correctors in the ring's straight sections near both collision points of circulating beams. The required characteristics and configuration of these correctors are optimized using a genetic algorithm. We find that thereby the aperture can be increased by a factor of ≈ 1.5–2 compared to the default value. This result is promising given that our simulation of beam dynamics is preliminary. At the next stage, we envisage taking additional factors into account, such as the uncertainties of magnetic fields, alignment of magnetic elements, orbit distortions, and coupling between betatron oscillations.

ACKNOWLEDGMENTS

This work was supported by the Russian Science Foundation under project no. 14-50-00080.

REFERENCES

1. V. D. Kekelidze, V. A. Matveev, I. N. Meshkov, A. S. Sorin, and G. V. Trubnikov, "Project nuclotron-based ion collider facility at JINR," Phys. Part. Nucl. **48**, 727–741 (2017).
2. O. Kozlov, A. Eliseev, H. Khodzhibagiyan, S. Kostromin, I. Meshkov, A. Sidorin, and G. Trubnikov, "Collider of the NICA accelerator complex: optical structure and beam dynamics," in *Proceedings of RUPAC2012, MOPPA017, St. Petersburg, Russia, 2012.*
3. The structure is provided by S. Kostromin.
4. https://atcollab.github.io/at/.
5. S. Glukhov, E. Levichev, S. Nikitin, P. Piminov, D. Shatilov, and S. Sinyatkin, "6D tracking with compute unified device architecture (CUDA) technology," in *Proceedings of ICAP 2015, Shanghai, China,* Paper WEP34.
6. H. Grote, F. Schmidt, L. Deniau, and G. Roy, The MAD-X program, Methodical Accelerator Design, Version 5.02.06, User's Reference Manual. http://madx.web.cern.ch/madx/.
7. A. E. Bolshakov, P. R. Zenkevich, and O. S. Kozlov, "Study of the asymptotic dynamic aperture in the NICA collider using symplectic tracking codes," Phys. Part. Nucl. Lett. **12**, 831–835 (2015).
8. S. A. Glukhov and E. B. Levichev, "Dynamic aperture optimization of the NICA collider," in *Proceedings of RuPAC2016, St. Petersburg, Russia, 2016,* Paper FRCAMH08.
9. E. B. Levichev and P. A. Piminov, "Analytic estimation of the non-linear tune shift due to the quadrupole magnet fringe field," arXiv:0903.3028 (2009).
10. B. D. Muratori, J. K. Jones, and A. Wolski, "Analytical expressions for fringe fields in multipole magnets," Phys. Rev. ST Accel. Beams 18, 064001 (2015); arXiv:1404.1762.
11. K. Oide and H. Koiso, "Dynamic aperture of electron storage rings with noninterleaved sextupoles," Phys. Rev. E **47** (2010).
12. A. Wolski, J. Gratus, and R. W. Tucker, "Symplectic integrator for s-dependent static magnetic fields based on mixed-variable generating functions," J. Instrum. **7**, 04013 (2012); arXiv:1206.6654.
13. M. Venturini and A. Dragt, "Accurate computation of transfer maps from magnetic field data," Nucl. Instrum. Methods Phys. Res. **427**, 387–392 (1999).
14. R. Baartman, "Intrinsic third order aberration in electrostatic and magnetic quadrupoles," in *Proceedings of the Particle Accelerator Conference, Vancouver, Canada, 1997.*

15. A. V. Bogomyagkov, E. B. Levichev, P. A. Piminov, A. Chance, B. Dalena, J. Payet, R. Maria, S. Fartoukh, and M. Giovannozzi, "Analysis of the non-linear fringe effects of large aperture triplets for HL-LHC project," in *Proceedings of IPAC'2013, Shanghai, China*, Paper WEPEA049.
16. G. H. Hoffstatter and M. Berz, "Symplectic scaling of transfer maps including fringe fields," Phys. Rev. E **54** (1996).
17. Lin Song, *NGPM—A NGSA-II Program in Matlab* (Aerospace Structural Dynamics Res. Laboratory, 2011).
18. K. Deb, A. Pratap, S. Agarwal, and T. Meyarivan, "A fast and elitist multiobjective genetic algorithm NSGA-IIJ," Evolut. Comput. **6**, 182–197 (2011).
19. N. Barricelli, "Esempi numerici di processi di evoluzione," Methodos, 45–68 (1954).
20. N. Barricelli, "Symbiogenetic evolution processes realized by artificial methods," Methodos, 143–182 (1957).
21. J. H. Holland, *Adaptation in Natural and Artificial Systems* (Univ. of Michigan Press, Ann Arbor, 1975).
22. A. S. Hofler, "Genetic algorithms and their applications in accelerator physics," in *Proceedings of the PAC 2013, Pasadena, CA,* Paper THTB1, pp. 1111–1115.
23. C. Sun, D. Robin, H. Nishimura, and C. Steier, "Dynamic aperture optimization using genetic algorithms," in *Proceedings of 2011 Particle Accelerator Conference, New York, NY, USA, 2011,* Paper TUON4.
24. N. Carmignani, L. Farvacque, S. M. Liuzzo, B. Nash, T. Perron, P. Raimondi, R. Versteegen, and S. White, "Linear and nonlinear optimization for the ESRF upgrade lattice," in *Proceedings of IPAC'2015, Richmond, VA, USA, 2015.*
25. M. P. Ehrlichman, "Genetic algorithm for chromaticity correction in diffraction limited storage rings," Phys. Rev. Accel. Beams **19**, 044001 (2016).
26. L. Wang, H. Xiaobiao, Yu. Nosochkov, J. A. Safranek, and M. Borland, "Optimization of the dynamic aperture for SPEAR-3 low-emittance upgrade," SLAC-PUB-15037 (2012).
27. Xavier Nuel Gavalda, *Multi-Objective Genetic based Algorithms and Experimental Beam Lifetime Studies for the Synchrotron SOLEIL Storage Ring* (Univ. Paris-Saclay, 2016).
28. A. Terebilo, "Accelerator toolbox for MATLAB," SLAC-PUB-8732 (2001).
29. https://matlab.ru/.
30. B. Nash, N. Carmignani, L. Farvacque, S. Liuzzo, T. Perron, P. Raimondi, R. Versteegen, and S. White, "New functionality for beam dynamics in accelerator toolbox (AT)," in *Proceedings of IPAC'2015, Richmond, VA, 2015.*

Translated by A. Asratyan